



Universidad Autónoma  
de Madrid

**Biblos-e Archivo**  
Repositorio Institucional UAM

**Repositorio Institucional de la Universidad Autónoma de Madrid**

<https://repositorio.uam.es>

Esta es la **versión de autor** del artículo publicado en:  
This is an **author produced version** of a paper published in:

Journal of the Electrochemical Society 166.6 (2019): D181-D188

**DOI:** <https://doi.org/10.1149/2.0321906jes>

**Copyright:** © 2019 The Electrochemical Society

El acceso a la versión del editor puede requerir la suscripción del recurso  
Access to the published version may require subscription

# Electrochemical co-deposition of gold and carbon nanocapsules from a colloidal suspension

A. Igual Muñoz<sup>1,\*</sup>, N. Alonso-Morales<sup>2</sup>, J. Palomar<sup>2</sup>, M. A. Gilarranz<sup>2</sup>, S. Mischler<sup>1</sup>

\* [anna.igualmunoz@epfl.ch](mailto:anna.igualmunoz@epfl.ch), +41 216937326, Ecole Polytechnique Fédérale de Lausanne, Tribology and Interface Chemistry Group, EPFL SCI STI SM, Station 12, CH-1015 Lausanne, Switzerland

<sup>1</sup> Ecole Polytechnique Fédérale de Lausanne, Tribology and Interface Chemistry Group, EPFL SCI STI SM, Station 12, CH-1015 Lausanne, Switzerland

<sup>2</sup> Chemical Engineering Department, Autónoma University of Madrid, Cantoblanco, 28049 Madrid, Spain

## Abstract

This paper shows the preparation of carbon nanocapsules and their co-deposition with gold from a colloidal galvanic bath on a nickel electrode to obtain gold/nanocapsules composite coatings. The incorporation of the nanocapsules was confirmed by surface analysis and confocal microscopy. The influence of suspension preparation, nanocapsule concentration and stirring during the co-deposition was analysed and showed that capsules strongly adhere on the surface and are coated by the gold matrix forming rounded clusters. The efficiency of the galvanostatic deposition increases in presence of capsules due to the increase in the active area and the metal growth on the carbon surfaces. The results establish a theoretical background for the electrochemical co-deposition of carbon nanocapsules acting as carriers for the further development of smart coatings.

## 1 Introduction

The production of composite coatings by electrolytic co-deposition of inert, semi-conductive, and conductive particles with metal from galvanic baths has been extensively studied in the past last decades and several review papers have been published in the field [1-3]. The interest shown in these composite deposits was due to their various intrinsic engineering

applications which allows for improving mechanical and physicochemical properties of the resulting material (i.e. corrosion and wear resistance). The type, size and number of incorporated particles depends on the final functionality desired for the composite coating. Due to the versatility and tailorability of this type composite materials the number of potential applications is continuously increasing, from technologies related to aerospace, sensors, automotive, electronics, memory devices, construction, energy to biomedical or other industries.

Among different particles, carbon is one of the first materials whose co-deposition was reported in literature [4], probably due to the combination of hydrophobicity and conductivity, which results in good co-deposition efficiency. More recently, carbon nanotubes (CNTs) have been used as important reinforcement components in various metallic, ceramic and polymeric materials to confer strength, toughness and wear/corrosion resistance due to their unique mechanical, thermal, electrical, optical and structural properties [5-6]. Indeed, electrodeposition of nickel coatings containing CNTs has been investigated extensively. Many studies have used CNTs because their advantageous mechanical, thermal and electrical properties enhance the surface properties of nickel coatings, while they have also been used as solid lubricant and strengthening phase [7-13].

Gold electrodeposition is widely used in the electronic industry due to its electrical and thermal conductivity, high ductility and excellent wear resistance and corrosion resistance. Gold is also known to be an excellent metal for wire bonding integrated circuits (ICs). However, lifetime of gold coatings is still a concern and the increase in durability of those gold coatings could be improved by incorporating solid particles into the metallic matrix. Different particles have been successfully incorporated to gold and gold alloy coatings via electrochemical co-deposition. Soft particles such as PTFE [14] were used to decrease the coefficient of friction, while ceramic particles such as  $\text{Al}_2\text{O}_3$  [15-16] or  $\text{B}_4\text{C}$  [17] to increase the hardness. Among the different particles used to increase the functionality of gold coatings, conductive carbon was also selected in order to increase the wear resistance and to guarantee the electrical conductivity of the resulting coating [18-19]. So far, co-deposition studies were focussed on the integration of solid particles aimed at improving selected mechanical properties. In the recent year, hollow particles have been made available as carriers for a number of functional substances ranging from corrosion inhibitors to dyes, or drugs. Incorporation of such particles into organic coating has led to the appearance of smart, self-healing surfaces. However, no attempt to incorporate such carriers in galvanic coatings

has been described since now. The aim of this work is to determine the co-deposition mechanisms of hollow carbon nanocapsules with gold as a function of processing parameters (deposition time, concentration of nanocapsules and agitation). This study should contribute establishing a theoretical background for the electrochemical co-deposition of carbon nanocapsules as carriers for the further development of smart coatings.

## 2 Materials and methods

### 2.1 Materials and reagents

Commercial acidic hard gold electrolyte containing 2 g/L of gold in form of  $\text{KAu}(\text{CN})_2$  and 0.35 g/L of Nickel was used for the electrochemical deposition tests. The pH of the electrolyte was 4.3.

The metallic substrate for the electrodeposition was a pure Nickel (99.9%) rod 12 mm in diameter.

The silica templates for the preparation of carbon nanocapsules were synthesized using tetraethylorthosilicate (TEOS) (98%) and octadecyltrimethoxysilane (C18TMS) (90%) purchased from Sigma–Aldrich. Absolute ethanol, ammonia (20%) and hydrofluoric acid (48%) were provided by PanReac Applichem. Resol resin (Bakelite ® PF9934 FL) was provided by Hexion Specialty Chemicals Iberica S.A.

### 2.2 Synthesis of carbon nanocapsules and suspension preparation

The carbon nanocapsules were synthesized following the templating method reported in previous works [20–22]. The silica template showed spherical morphology and was composed of a non-porous core and a mesoporous shell. In the synthesis of the template, 15 mL of TEOS was added to a reaction medium formed by 12.6 mL of 20% aqueous ammonia solution, 185 mL of absolute ethanol and 20.3 mL of deionized water. The mixture was maintained at 303 K with vigorous stirring during 1 h to achieve the formation of the non-porous cores. A mixture containing 12.5 mL of TEOS and 5 mL of C18TMS was added to the colloidal solution containing the silica cores to form the silica mesoporous shell around them by reaction under gentle stirring at 303 K. After one hour of reaction, an additional 12.5 mL aliquot of the TEOS and 5 mL of C18TMS mixture was added and let react for one hour

to further increase the thickness of the silica mesoporous shell. The template particles synthesized were isolated by filtration and calcined at 823 K for 6 h under air atmosphere.

A commercial resol resin was used as carbon precursor in a mass ratio of 3 g of resol resin per g of template. The resin was dissolved in 100 mL of absolute EtOH and this solution was infiltrated into the template in a rotary vacuum evaporator at 100 mbar and 40 °C until dryness. Then, the resin was cured by heating the sample at 130 °C for 1h in air. The cured resin-silica composite was treated at 700 °C for 1 h, using a temperature ramp of 5 °C min<sup>-1</sup>, in an inert atmosphere of N<sub>2</sub>. The silica template was removed by washing it with 48% hydrofluoric acid. The resulting carbon nanocapsules were washed with deionized water until neutrality and dried at 373 K for 24 h.

The porous texture of the carbon nanocapsules was characterized by N<sub>2</sub> adsorption/desorption isotherms at 77 K in a TriStar II 3020 (Micromeritics) system after degassing at 423 K under vacuum (~0.1 mbar) for a minimum of 6 h. The surface area was calculated using the Brunauer-Emmet-Teller (BET) equation. The mesopore size distribution was calculated by the Barrett-Joyner-Halenda (BJH) method from the adsorption branch. The morphology was studied by scanning electron microscopy (SEM) in a Hitachi S-3000N microscope and transmission electron microscopy (TEM) using a JEM 2100 microscope.

The obtained nanocapsules in form of powder were dispersed in 50 ml of gold bath adding some drops of ethanol and sonicating during 15 minutes in a Branson Ultrasonics Sonifier in order to obtain suspensions with 0.5 g/L and 0.25 g/L of carbon nanocapsules. The resulting suspension was analysed by laser diffraction in a Malvern Mastersizer instrument.

### 2.3 Electrochemical co-deposition procedure

Electrochemical co-deposition of gold and nanocapsules was carried out on a rotating disk electrode from the commercial gold bath with dispersed nanocapsules under galvanostatic conditions at an applied constant current density of -1.7 mA/cm<sup>2</sup>. The co-deposition was carried out at different rotation rates (static, 100, 500 and 900 rpm) in the colloidal bath at 30 °C. A nickel electrode disk with an exposed area of 1.13 cm<sup>2</sup> was used as the working electrode. The counter-electrode was a platinum wire and a saturated calomel electrode reference (0.196 V vs SHE) was used in a three-electrode configuration cell. An Autolab PGSTAT30 potentiostat allowed for performing all electrochemical tests.

Cathodic polarization curves were also carried out from the Open Circuit Potential (OCP) to -1.2 V<sub>SCE</sub> at 2 mV/s.

The current efficiency was determined by Electrochemical Quartz Crystal Microbalance (EQCM) measurements on gold coated quartz crystals (AT-cut 10 MHz) of 23 mm<sup>2</sup> surface area. The electrochemical cell with 3-electrode configuration described previously was also used with the gold coated quartz crystal as working electrode. All tests were carried out at 30°C under stagnant conditions and in direct contact with air. Additional details of the experimental set-up are given elsewhere [23].

Two replica of all tests under the same conditions were carried out in order to check for the reproducibility of the data.

## 2.4 Surface characterization

A Keyence laser scanning confocal microscope (VK-X250) was used for characterizing the surface topography and a Scanning electron microscope (SEM Phillips XLF30) and an Electron X-ray spectrometer (EDS) were used to determine the surface morphology and the elemental composition of the composite coating.

Cross-section of the obtained coatings were carried out using Focus-Ion-Beam and high resolution field emission SEM (Zeiss XB540). The surface was milled with a Ga<sup>+</sup> ion beam.

# 3 Results

## 3.1 Nanocapsule size and characterization

The carbon nanocapsules showed a homogeneous morphology consisting of spherical particles with average diameter of 550 nm (Figure 1.A). The TEM image (Figure 1.B) shows that the capsules have a hollow spherical nucleus with an average diameter of 370 nm and a homogeneous shell with a thickness of 90 nm. Therefore, they were obtained successfully as the inverse replica of the silica template. The SEM image also shows that some of the nanocapsules seem to form agglomerates of 2-4 units. The carbon nanocapsules showed a BET specific surface area of 1541 m<sup>2</sup>/g with a total pore volume of 1.75 cm<sup>3</sup>/g, which is a contribution of both micro and mesopores.

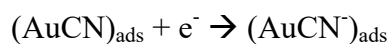
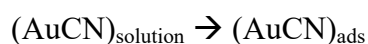
### 3.2 Dispersability of the nanocapsules in the electrolytic bath

Figure 2 shows an example of the particle size distribution of a gold suspension containing 0.5 g/L of carbon nanocapsules. The obtained suspension shows a uniform particle distribution with an average diameter of around 3  $\mu\text{m}$ , higher than the diameter of a single nanocapsule. This means that during the suspension process of the nanocapsules there is some agglomeration which is not possible to disperse with the mechanical action of the sonication. In addition to this, some of the agglomeration may occur during the synthesis of the nanocapsules, as suggested by the electron microscopy images in Figure 1.

Although not shown here, addition of 0.1% of nonionic surfactant (Tween 20) did not improve the dispersability of the nanocapsules in the aqueous galvanic bath.

### 3.3 Electrochemical co-deposition

Two examples of cathodic polarization curves in the Au and Au-0.25 g/L C baths at two different rotation rates are shown in Figure 3. All curves show an initial exponential increase in current (in absolute value) with the applied potential due to a charge transfer control mechanism, and a cathodic peak around -0.9  $V_{\text{SCE}}$  which depends on the rotation rate. Such peak is not related to the diffusion control of the  $\text{Au}(\text{CN})_2^-$  nor the HER (hydrogen evolution reaction). It is likely that the peak is related to the reduction of AuCN adsorbed on electrode surface [24]. The AuCN species adsorb on the surface rather than  $\text{AuCN}^-$  soluble species. Therefore, gold electrodesposition occurs via reduction of adsorbed AuCN followed by the charge transfer step:



At more negative potentials, when the current density increases abruptly, the electrochemical deposition of gold was governed by the following direct charge transfer reaction [25]:



Furthermore, this region is also governed by the hydrogen evolution reaction (reduction of water).

In presence of nanocapsules, slightly lower current densities were measured during the cathodic scan.

Electrochemical deposition of Au and co-deposition of Au+nanocapsules was carried out under the same galvanostatic conditions of constant applied current density of  $-1.7 \text{ mA/cm}^2$  during 2250 s. Under these conditions, in both cases the system is controlled by the primary current distribution, thus determined by its geometry and the conductivity of the electrolyte. During the deposition, the potential was constant after the first 100 seconds and slightly lower in the Au bath compared to the value measured using the colloidal suspension. In any case, the differences in the resulting potential were small, and all of them laid around 1000 mV.

### 3.4 Efficiency of the electrochemical co-deposition

EQCM measurements were carried out to quantify the efficiency of the deposition and the underlying mechanisms. Figure 4 shows the potential and the mass evolution with time of the gold quartz crystal during galvanostatic deposition at  $-1.7 \text{ mA/cm}^2$  in two different electrolytic baths, the pure gold and the suspension containing carbon capsules. It is possible to observe that the potential remains constant during the whole deposition period while the mass linearly increases with time. A Higher mass was deposited from the suspension bath (up to 30%), which means higher efficiency in the gold deposition in presence of carbon capsules (mass contribution of capsules incorporation into the metal matrix is negligible compared to weight of gold).

The current efficiency for the electrodepositions under the studied conditions was determined from the electrochemical charge supplied during the deposition and the measured mass using Faraday's law. From those values, an average current efficiency of 30% was obtained for the gold electrodeposition and 40% for the co-deposition of gold and carbon capsules.

### 3.5 Coating characterization

Morphology of the obtained coatings was studied by microscopic techniques. Figure 5 shows an example of the optical and confocal 3-D images of the composite coatings obtained at different rotation rates in a gold suspension containing 0.25 g/L of C nanocapsules. It is possible to observe how clusters of particles are covered by gold forming a rounded pattern



on the whole surface. From the images, the percentage of surface covered by clusters, the maximum height of the clusters and their average circular diameter (assuming the clusters to be spheres) was obtained by image analysis and the results are summarized in Table 1. The average circular diameter matches very well with the average particle size obtained from the laser diffraction measurements with values between 2.16 and 3.41  $\mu\text{m}$ (Figure 2).

Figure 6 shows a FIB cross-section of one composite coating obtained from the bath Au+0.25 g/L C after galvanostatic deposition at  $-1.7 \text{ mA/cm}^2$  during 2250 s. It is clearly seen how below the rounded shape, clusters of 3-4 nanocapsules are perfectly incorporated under the Au layer. Likewise, the original morphology of nanocapsules can be clearly distinguished indicating their stability under the deposition conditions.

In order to gain a better understanding of the co-deposition mechanism of gold and the nanocapsules, the evolution of the morphology as a function of charge density (deposition time) was studied by confocal microscopy and SEM at a constant applied current density. The results shown in Table 1 indicate that surface coverage increases with the deposition time, while the average height of the clusters is independent of the duration of the galvanic deposition. On the other hand, the agglomeration of incorporated clusters increases with deposition time, resulting in a slightly higher average circular diameter of those clusters. The highest coverages of 77-88% were obtained for the highest rotation rate (900 rpm).

From the SEM images, it is possible to observe that at short times, Figure 7(a), the nickel surface was already covered by gold and some clusters adsorbed on it. Figure 7(b) shows a detail of some clusters with different gold coverage of a composite coating obtained after 600 s of galvanostatic deposition. Non-covered capsules were also distinguished. The instantaneous nucleation and 3D cylindrical growth of the gold on the carbon nanocapsules as already reported [26] was appreciated from the beginning of the depositions. At longer times, Figure 7(c-d) and Figure 7(e-f), most of the clusters of nanocapsules are covered by the metallic gold forming a cauliflower morphology. The EDX analysis of the surface showed that less Ni was incorporated on the top of C nanocapsules.

For comparison purposes the appearance of the gold coating after electrochemical deposition at  $-1.7 \text{ mA/cm}^2$  after 2250 s is shown in Figure 8. The gold coating shows also a globular growth of the metal matrix with the absence of the clusters. There is a change in coating morphology from a rounded one in the pure gold coating to a cauliflower morphology due to

the growth disturbance caused by the presence of carbon nanocapsules at the surface of clusters, and as these clusters begin to co-deposit due to their incorporation.

The adsorption of the conductive carbon capsules onto the surface change the active area for the electrochemical co-deposition. This active area was quantified assuming the clusters are hemispheres and measuring the average height of the clusters and their equivalent diameter, as it can be seen in Table 1. From those values, the electrochemically active area was determined as a function of deposition time and shown in Figure 9, following a perfect linear trend.

The change in the active area for gold electrodeposition in presence of carbon capsules modifies the amount of gold per surface area covering the surface, and hence the thickness of gold co-deposited with the capsules. The thickness of the coatings can be calculated by assuming that the main contribution of the mass comes from the gold deposition, thus dividing the increase in mass measured by EQCM and shown in Figure 4 by the gold density ( $19.3 \text{ g/cm}^3$ ). Accordingly, Figure 10 shows the evolution with time of the gold and composite coating thickness when the increase in area due to the incorporation of the capsules (Figure 9 is considered. For comparison purposes the thickness of the composite coating without the area correction is also shown in the figure. It is possible to observe that the thickness of the composite coating linearly increases at the beginning of the test (the first 400 seconds), and at longer deposition times the slope changes towards lower values. This means that during the co-deposition there is an initial gold deposition on the nickel surface followed by the adhesion of the capsules and the modification of gold deposition due to the presence of the carbon capsules. This modification causes a decrease in the final gold thickness on the whole active surface. This is in good agreement with the morphological results of the composite coatings, whose average height did not significantly change with the deposition time, as it can be seen in Table 1.

## 4 Discussion

### 4.1 Co-deposition mechanisms

Gold composites formation has been reported to involve adsorption of ionic species on the surface of the particles in the galvanic bath, diffusion of the charged particles to the cathode, reduction of the adsorbed ions and strong anchoring of the particles to the cathode surface

[27]. Incorporation of carbon nanocapsules into gold can be then described with a three-step model based on the previously proposed by Eroglu et al. [28] and shown in Figure 11: (1) mass transfer of the particles to the electrode surface, (2) adhesion of the capsules onto the surface and (3) incorporation in the growing gold film by gold salt reduction on the capsule surface. In this system where conductive particles are co-deposited with the metal, when the carbon capsules reach the metal surface, they are strongly trapped and gold salt reduces on the whole capsule surface. There is not a burial mechanism by the growing metal coating but a direct reduction of the gold on the adhered capsule surface, which makes the incorporation rate much higher than that observed for non-conductive particles [28]. On the other hand, the typical hydrophobic properties of the carbon capsules also favour the gold to be adsorbed onto the carbon surface, thus enhancing its reduction under galvanostatic conditions.

In general, at the considered applied current density for the galvanostatic depositions, the current distribution is governed by the geometry of the system, thus uniformly covering the 3-D structure of the capsules clusters.

Taking into account all above considerations, the proposed model was applied by using the parameters showed in Table 2.

The only parameter which has been changed in the present co-deposition of conductive particles, compared to the one used for the SiC particles [28-29], is the incorporation rate ( $k_{inc}$ ). This incorporation rate was determined by considering the experimental results of the capsules incorporation (through the image analysis of the surfaces) shown in Figure 12 as a function of deposition time. In the model, the incorporation of the particles is considered as an incorporation rate, thus independent on the deposition time. This assumption differs from the experimental results because of the conductive character of the carbon particles, thus their different surface properties towards Au deposition.

With the parameters shown in Table 2, the influence of mass transport on the capsule incorporation in the coating was studied and the comparison between the experimental results and the predicted ones by the model are shown in Figure 13.

It is possible to observe that the model predicts quite well the experimental results. Only at 500 rpm the errors are higher. This effect of mass transport was already observed by Eroglu et al. [29] for SiC particle incorporation on a Nickel coating. At low rotation rate, mass-transfer limitations played a significant role and affect surface coverage, resulting in a nonlinear dependence of capsule incorporation rate and rotation rate.

## 5 Conclusions

Hollow carbon nanocapsules were fabricated and co-deposited on a nickel substrate from an electrolytic commercial hard gold bath. Co-deposition mechanisms were found to imply three successive steps: mass transfer of the capsules to the electrode surface, adsorption/adherence of the capsule on the surface and, finally, anchoring of the capsule by the gold electro deposition directly on the capsule surface. This mechanism differs in the last step to previously proposed mechanisms involving non conductive particles that are buried by the metal growing on the active electrode area around the particle. The metal film growth directly on the capsule surface makes the incorporation rate much higher than that observed for non-conductive particles. The model allowed rationalizing the influence of particle concentration and mass transport conditions in the particle incorporation in the coating.

**Acknowledgements:** This research has been financially supported by the Swiss Innovation Agency-Innosuisse within the frame of the CTI project 18738.1 PFNM-NM.

## 6 References

1. F. C. Walsh, C. Ponce de Leon A review of the electrodeposition of metal matrix composite coatings by inclusion of particles in a metal layer: an established and diversifying technology *Transactions of the IMF* **92**, 83 (2014).
2. A.K. Chaudhari, V.B. Singh A review of fundamental aspects, characterization and applications of electrodeposited nanocrystalline iron group metals, Ni-Fe alloy and oxide ceramics reinforced nanocomposite coatings *Journal of Alloys and Compounds* **751**, 194 (2018).
3. C. Janůky, E. Kecsenvity, K. Rajeshwar Electrodeposition of Inorganic Oxide/Nanocarbon Composites: Opportunities and Challenges *Chem ElectroChem* **3**, 181 (2016).

- 337 4. C. G. Fink and J. D. Prince, *Trans. Am. Electrochem. Soc.*, **54**, 315 (1928)
- 338 5. T. Casagrande, G. Lawson, H. Li, J. Wei, A. Adronov, I. Zhitomirsky  
339 Electrodeposition of composite materials containing functionalized carbon nanotubes, *Mater.*  
340 *Chem. Phys.*, **111**, 42 (2008).
- 341 6. M. Attarchi and S. K. Sadrnezhad Pulse reverse electrodeposition of spherical Ni-  
342 MWCNT composite skein, *IJE Trans. B*, **22B**, 161 (2009).
- 343 7. C. R. Carpenter, P. H. Shipway and Y. Zhu Electrodeposition of nickel-carbon  
344 nanotube nanocomposite coatings for enhanced wear resistance, *Wear*, **271**, 2100 (2011).
- 345 8. S. Arai, A. Fujimori, M. Murai and M. Endo Excellent solid lubrication of  
346 electrodeposited nickel-multiwalled carbon nanotube composite films, *Mater. Lett.*, **62**, 3545  
347 (2008).
- 348 9. X.H. Chen, C.S. Chen, H.N. Xiao, H.B. Liu, L.P. Zhou, S.L. Li and G. Zhang Dry  
349 friction and wear characteristics of nickel/carbon nanotube electroless composite deposits,  
350 *Tribol. Int.*, **39**, 22 (2006).
- 351 10. B.-G. An, L.-X. Li and H.-X. Li Electrodeposition in the Ni-plating bath containing  
352 multi-walled carbon nanotubes, *Mater. Chem. Phys.*, **110**, 481 (2008).
- 353 11. Y. S. Jeon, J. Y. Byun and T. S. Oh Electrodeposition and mechanical properties of  
354 Ni-carbon nanotube nanocomposite coatings, *J. Phys. Chem. Solids*, **69**, 1391 (2008).
- 355 12. C. R. Carpenter, P. H. Shipway and Y. Zhu The influence of CNT co-deposition on  
356 electrodeposit grain size and hardness, *Surf. Coat. Technol.*, **205**, 5059 (2011).
- 357 13. S. Iijima Helical microtubules of graphitic carbon, *Nature*, **354**, 56 (1991).
- 358 14. M. Rezrazi, M.L. Doche, P. Berbecot, J.Y. Hihn Au-PTFE composite coatings  
359 elaborated under ultrasonic stirring *Surface & Coatings Technology* **192**, 124 (2005).
- 360 15. C. Buelens, J.P. Celis, J.R. Roos Electrochemical aspects of the co-deposition of gold  
361 and copper with inert particles *Journal of Applied Electrochemistry* **13**, 541 (1983).
- 362 16. F. Wünsche, A. Bund W. Plieth Investigations on the electrochemical preparation of  
363 gold-nanoparticle composites *J Solid State Electrochem* **8**, 209 (2004).
- 364 17. B. Bozzini, B. Brevaglieri, P. L. Cavallotti, G. Giovannelli, S. Natali Hydrodynamic  
365 problems related to the electrodeposition of AuCu/B4C composites *Electrochimica Acta* **45**,  
366 3431 (2000) .

- 367 18. P. Cojocar, M. Santoro, A. Vincenzo, P.L. Cavallotti Properties of ECD Gold  
368 Composite with Nanostructured Carbon-Based Materials *ECS Transactions*, **3**, 15 (2007).
- 369 19. P. Cojocar, A. Vincenzo, P.L. Cavallotti Electrodeposition of Au/nanosized diamond  
370 composite coatings *J Solid State Electrochem* **9**, , 850 (2005).
- 371 20. N. Alonso-Morales, M.A. Gilarranz, J. Palomar, J. Lemus, F. Heras, J.J. Rodriguez,  
372 *Carbon* **59**, 430 (2013).
- 373 21. N. Alonso-Morales, Cristina Ruiz-Garcia, Jose Palomar, Francisco Heras, Luisa  
374 Calvo, Juan J. Rodriguez, and Miguel A. Gilarranz. *Ind. Eng. Chem. Res.* **56**, 7665 (2017).
- 375 22. R. Santiago, J. Lemus, D. Moreno, C. Moya, M. Larriba, N. Alonso-Morales, M.A.  
376 Gilarranz, J.J. Rodríguez, J. Palomar. *Chemical Engineering Journal* **348**, 661 (2018).
- 377 23. C. Valero Vidal, A. Igual Munoz, C.O.A. Olsson, S. Mischler Passivation of a  
378 CoCrMo PVD Alloy with Biomedical Composition under Simulated Physiological  
379 Conditions Studied by EQCM and XPS *Journal of the Electrochemical Society* **159**, C233  
380 (2012).
- 381 24. E.T. Eisenmann, Kinetics of the Electrochemical Reduction of Dicyanoaurate *Journal*  
382 *of the Electrochemical Society* **125**, 717 (1978).
- 383 25. L. Santinacci, T. Djenizian, P. Schwaller, T. Suter, A. Etcheberry and P. Schmuki  
384 Selective electrochemical gold deposition onto p- Si (1 0 0) surfaces *J. Phys. D: Appl. Phys.*  
385 **41**, 175301 (2008).
- 386 26. Y.G.Uand, A.Lasia Electrodeposition of Hard Gold from Acidic Solution *J.*  
387 *Electrochem. Soc.* **144**, 1979 (1997).
- 388 27. C. Larson Electrodespoited gold composite coatings Mechanism of formation,  
389 mechanical and tribological properties *Gold Bulletin* **17**, 86 (1984)
- 390 28. D. Erogluz, A.C. West Mathematical Modeling of Ni/SiC Co-Deposition in the  
391 Presence of a Cationic Dispersant *Journal of The Electrochemical Society*, **160**, D354 (2013).
- 392 29. D. Eroglu, A. Vilinska, P. Somasundaran, A. C. West Effect of a Cationic Polymer,  
393 Polyethyleneimine, on Ni/SiC Co-Deposition *Journal of The Electrochemical Society*, **160**,  
394 D35 (2013).

395

396

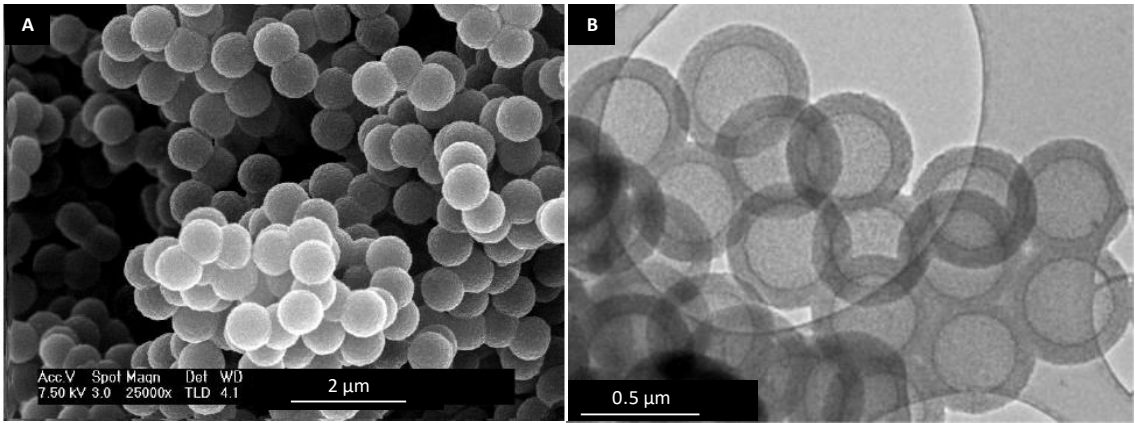
Table 1. Morphological parameters of the composite coatings obtained under different electrodeposition conditions

[Capsules] g/L	Agitation (rpm)	Deposition time (s)	Surface coverage %	Avg. height ( $\mu$ m)	Avg. circular diameter ( $\mu$ m)
0.25	100	600	10	1.79	2.31
		1400	40	1.56	2.78
		2250	53	1.73	2.94
	500	2250	40	2.61	3.22
	900	750	18	1.48	2.16
		2250	77	1.95	3.41
0.5	100	2250	49	1.23	2.88
	500	2250	32	1.47	2.75
	900	2250	88	1.13	2.89

Table 2. Values of the parameters used in the model

Parameter	Value
<b>K</b> (cm <sup>3</sup> /mol)	10 <sup>5</sup>
<b>a</b> (A/cm <sup>2</sup> )	0.16
<b>b</b> (rad/s)	54
<b>k<sub>inc</sub></b> (particles cm <sup>5</sup> /A <sup>2</sup> )	2 10 <sup>-7</sup>

405

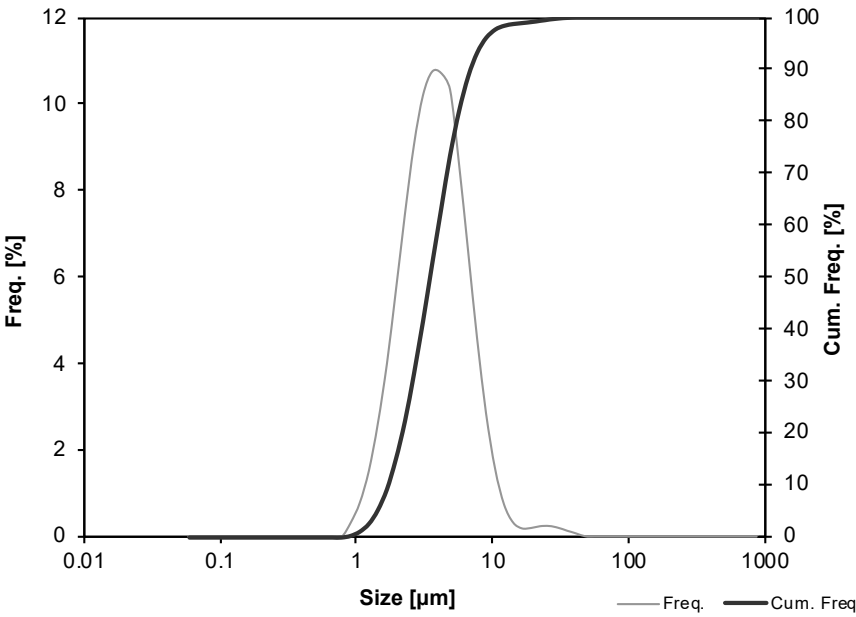


406

407

Figure 1. SEM (A) and TEM (B) images of the synthesized carbon nanocapsules.

408



409

410

Figure 2. Particle size distribution in the Au+0.5g/L C suspension

411



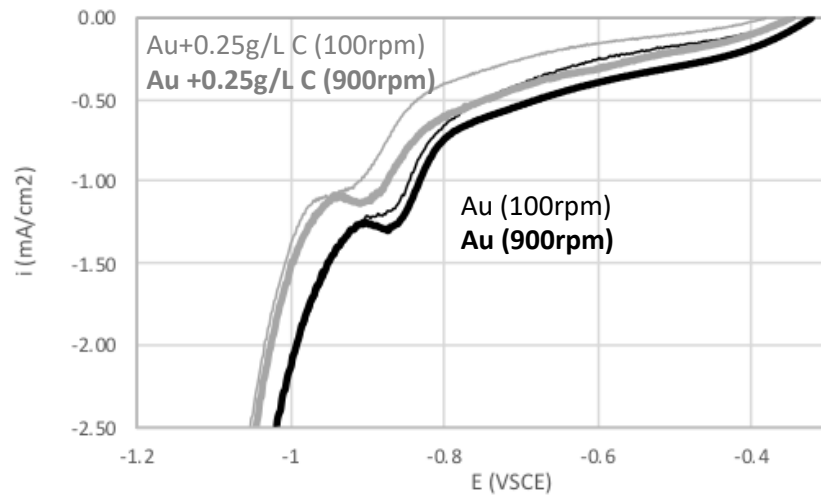
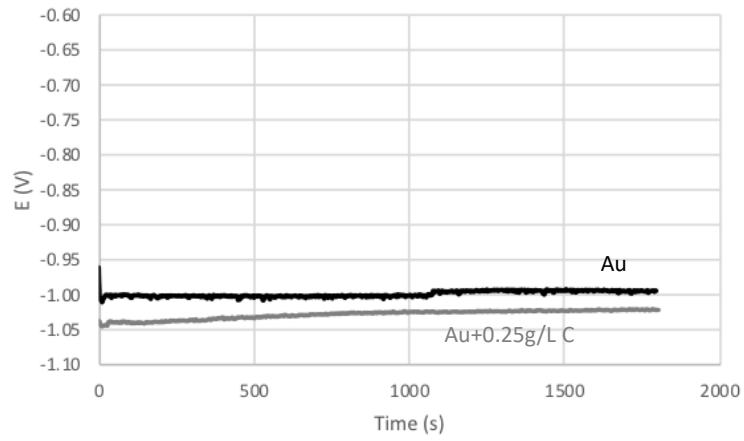


Figure 3. Cathodic polarization curves of the Au and the colloidal suspension Au+0.25 g/L C nanocapsule content.



(b)

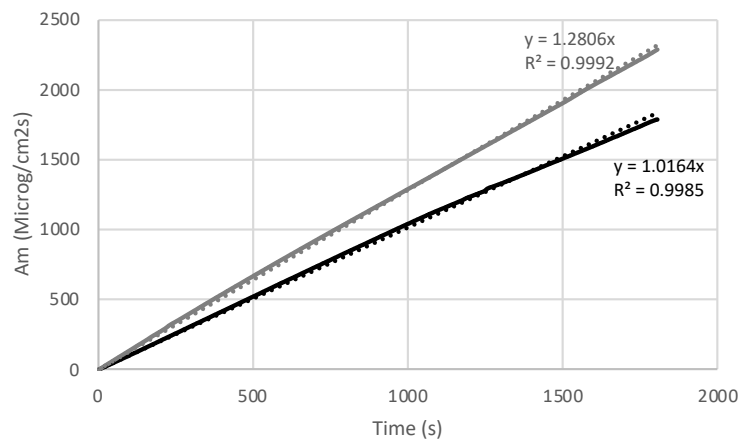
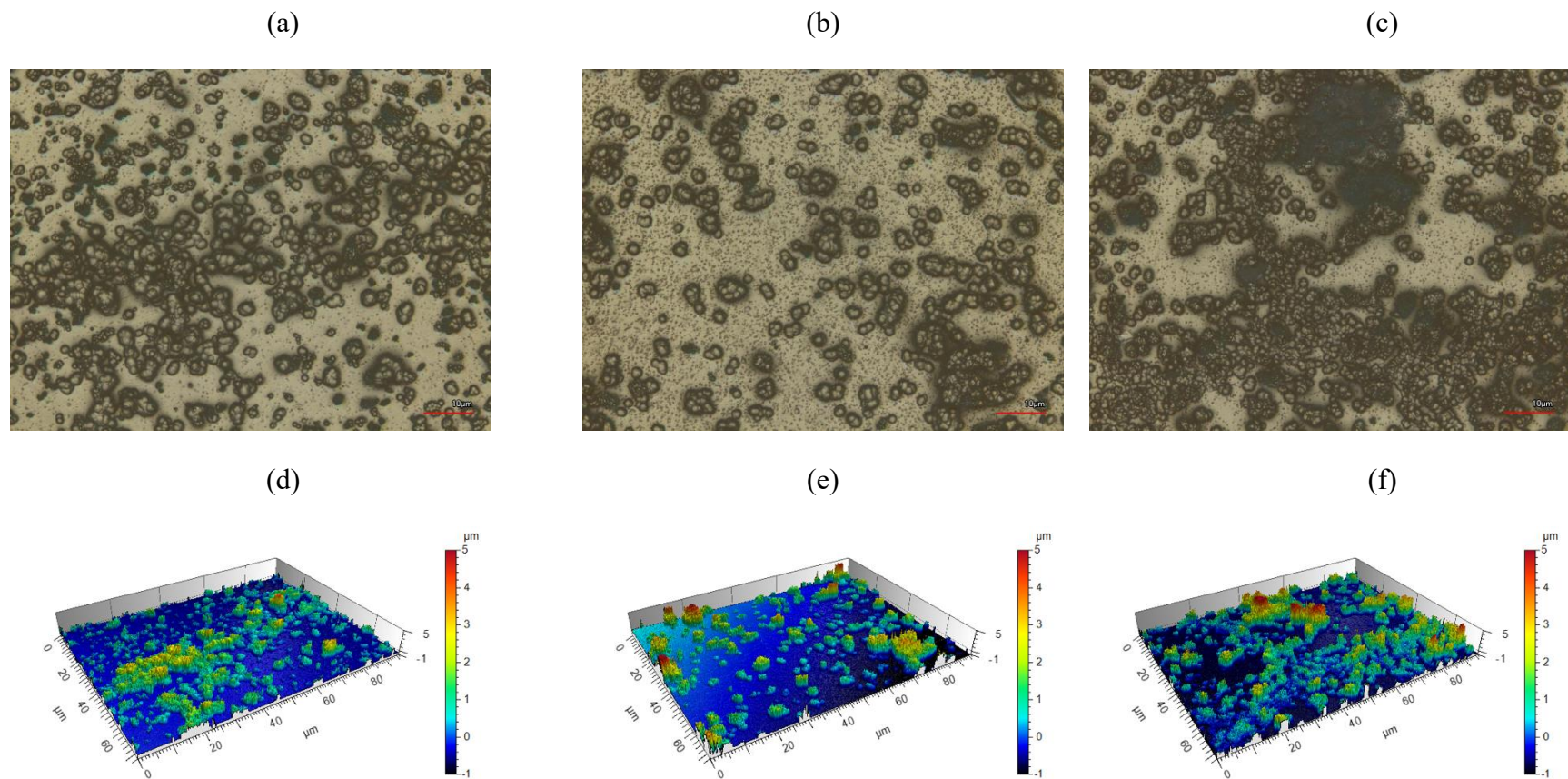


Figure 4. a) Potential and b) mass evolution with time at an applied current density of -1.7 mA/cm<sup>2</sup> in Au and Au+0.25 g/L C nanocapsules solutions.



440 Figure 5. Optical and confocal and 3D images of the coating composites 0.25 g/L C obtained at a constant current density of  $-1.7 \text{ mA/cm}^2$  at  
 441 different rotation rates: (a,d) 100 rpm, (b,e) 500 rpm and (c,f) 900 rpm  
 442

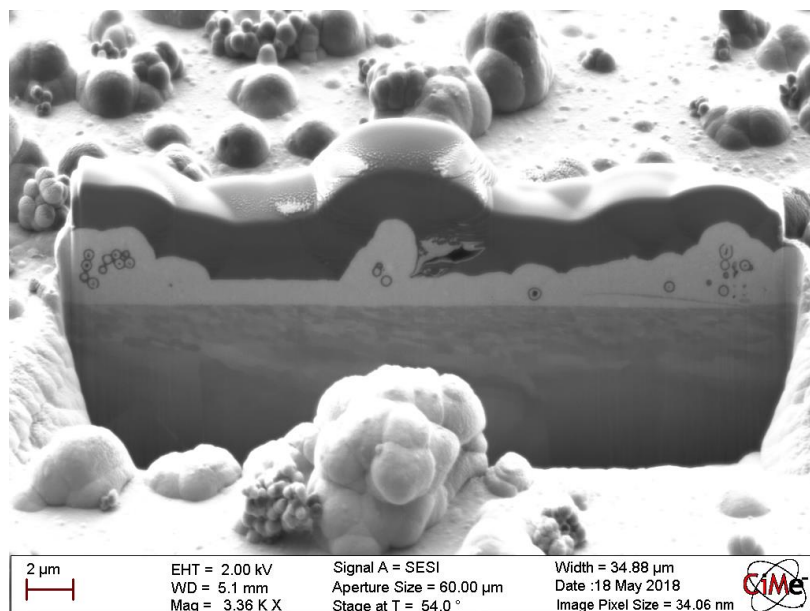
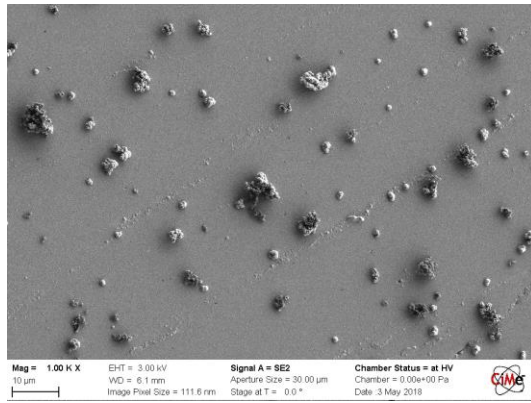
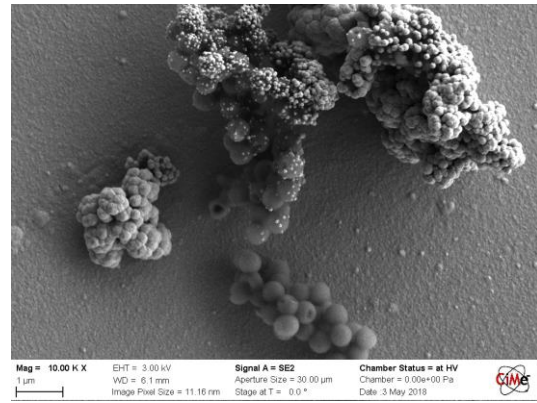


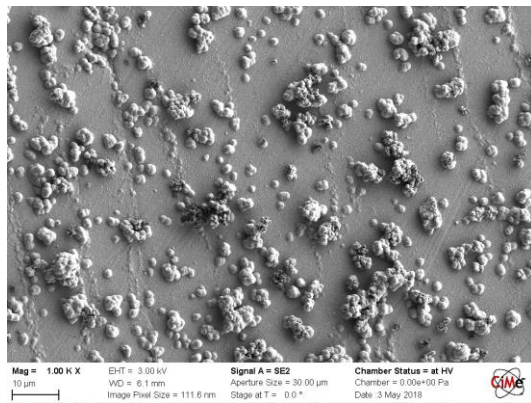
Figure 6. FIB cross section of the coating composite 0.25 g/L C obtained at a constant current density of  $-1.7 \text{ mA/cm}^2$



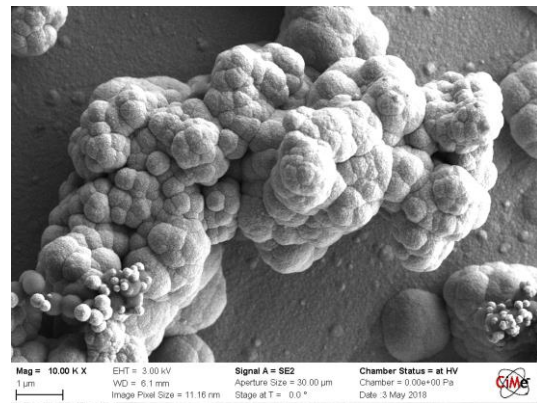
(a)



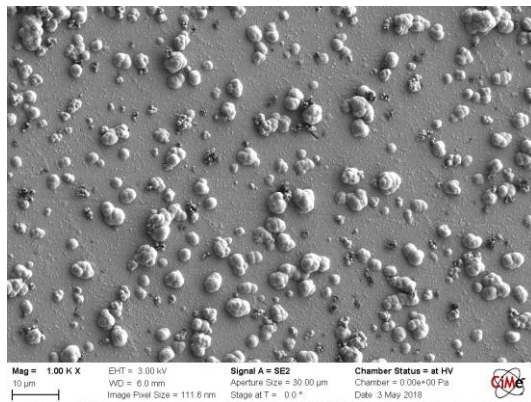
(b)



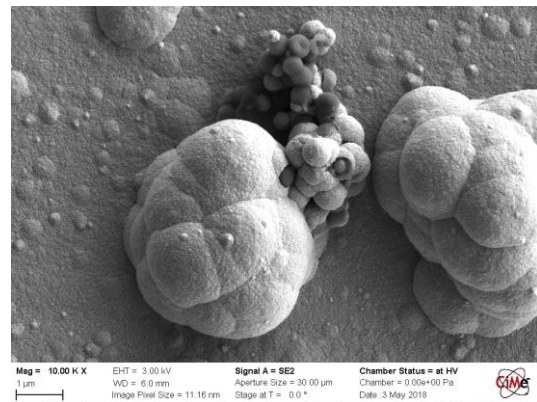
(c)



(d)



(e)



(f)

456 Figure 7. SEM images of the coating composites obtained at a constant current density of -1.7  
457 mA/cm<sup>2</sup> at different deposition times: (a-b) 600s, (c-d) 1400s and (e-f) 2250 s.

458



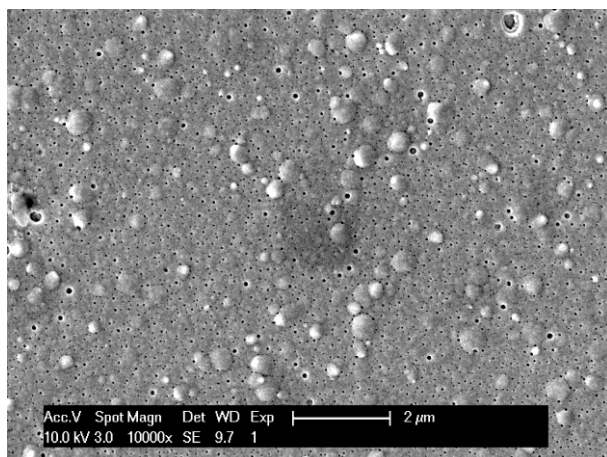


Figure 8. SEM images of the gold coating obtained at a constant current density of  $-1.7 \text{ mA/cm}^2$  during 2250 s.

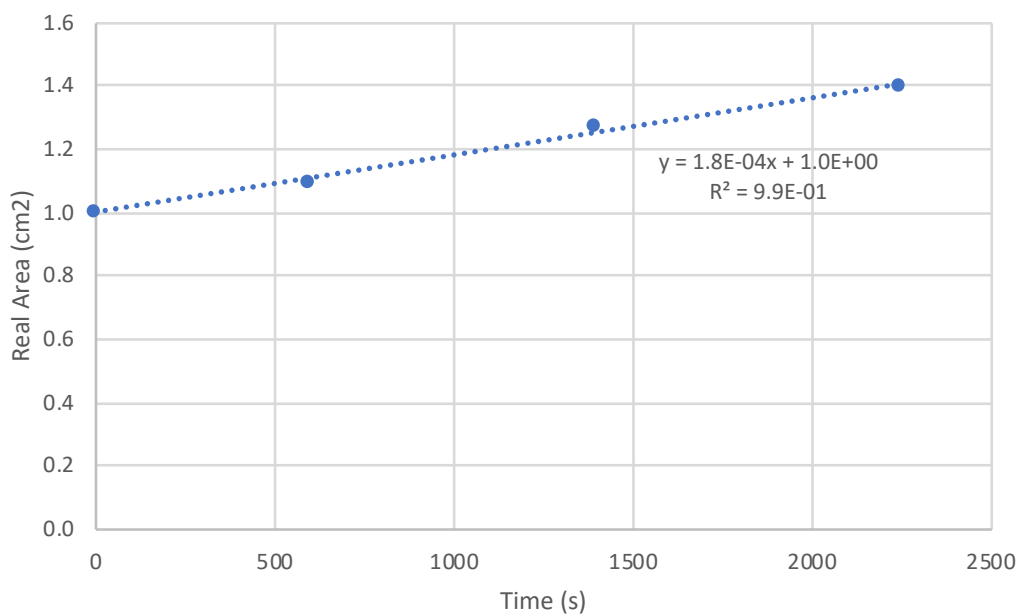


Figure 9. Linear increase of active area of the electrode as a function of deposition time

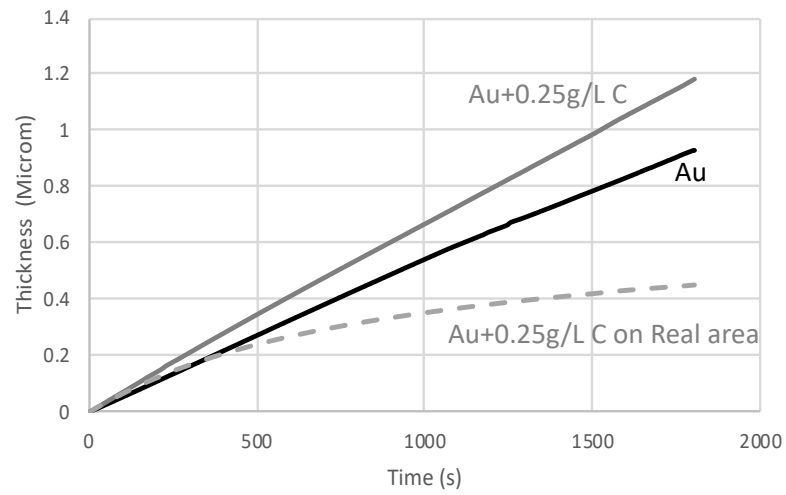


Figure 10. Variation of gold thickness with deposition time in the Au and Au+0.25 g/L C nanocapsules suspension taking into account the change in active area caused by the carbon nanocapsules incorporation.

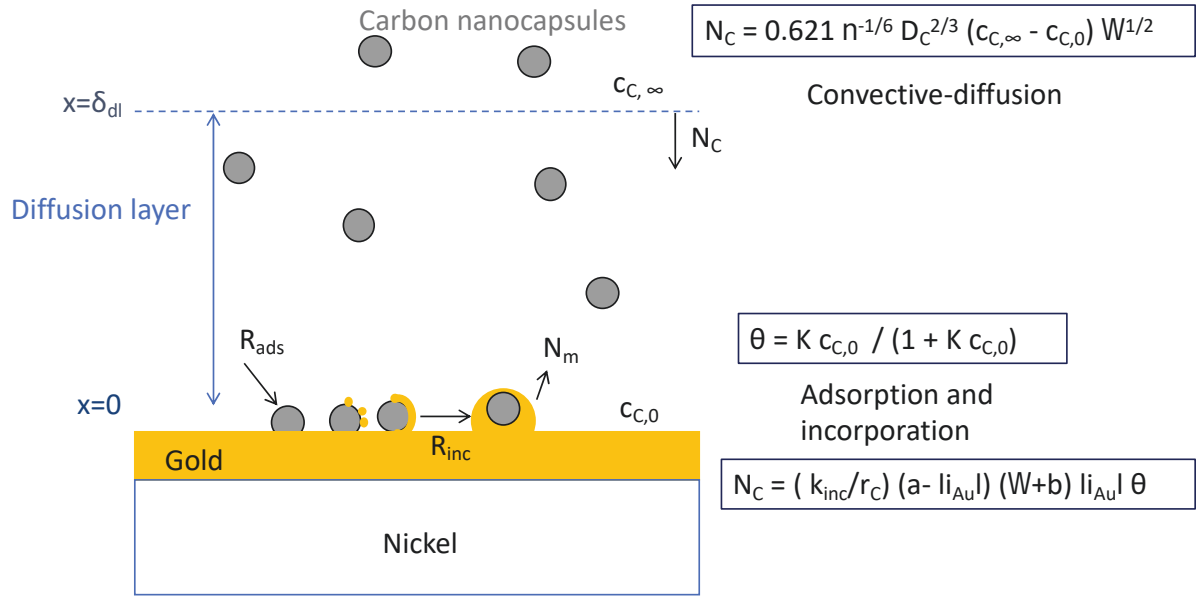


Figure 11. Adapted from [28] where  $N_c$  is the particle flux (particle/cm<sup>2</sup>s),  $\nu$  the kinematic viscosity of the electrolyte (cm<sup>2</sup>/s),  $D_C$  de diffusion coefficient of the particles (cm<sup>2</sup>/s),  $c_{C,\infty}$  the bulk concentration of the particles (particles/cm<sup>3</sup>,  $c_{C,0}$  the surface concentration of the particles (particles/cm<sup>3</sup>,  $\Omega$  the rotation speed (rad/s),  $\theta$  the surface coverage,  $K$  the Langmuir adsorption constant (cm<sup>3</sup>/mol),  $k_{inc}$  the incorporation rate constant (particles cm<sup>5</sup>/A<sup>2</sup>,  $r_C$  the particle radius (cm),  $a$  a constant (A/cm<sup>2</sup>,  $i_{Au}$  the current density for gold deposition (A/cm<sup>2</sup> and  $b$  a constant (rad/s).

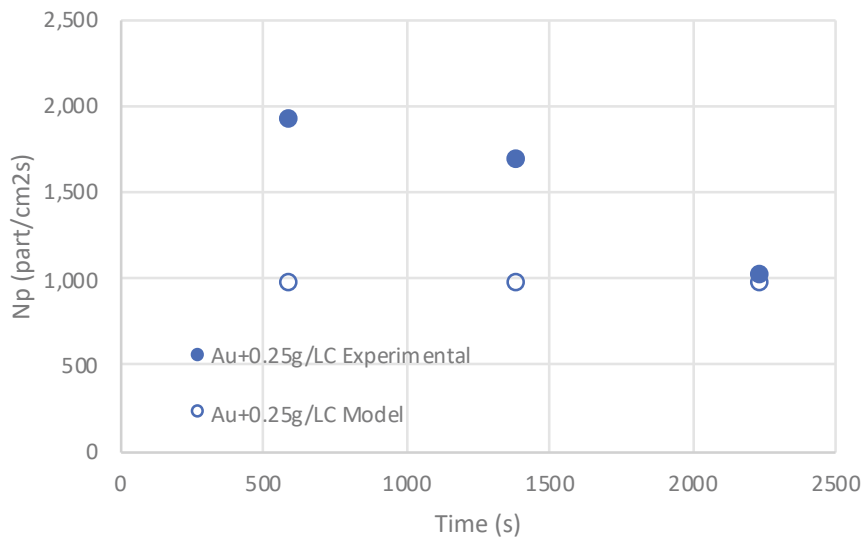




Figure 12. Experimental and predicted incorporation rate by the model as a function of time of the carbon particles with a bulk concentration of 0.25 g/L of C nanocapsules at a current density of  $-1.7 \text{ mA/cm}^2$  and RDE 100 rpm.

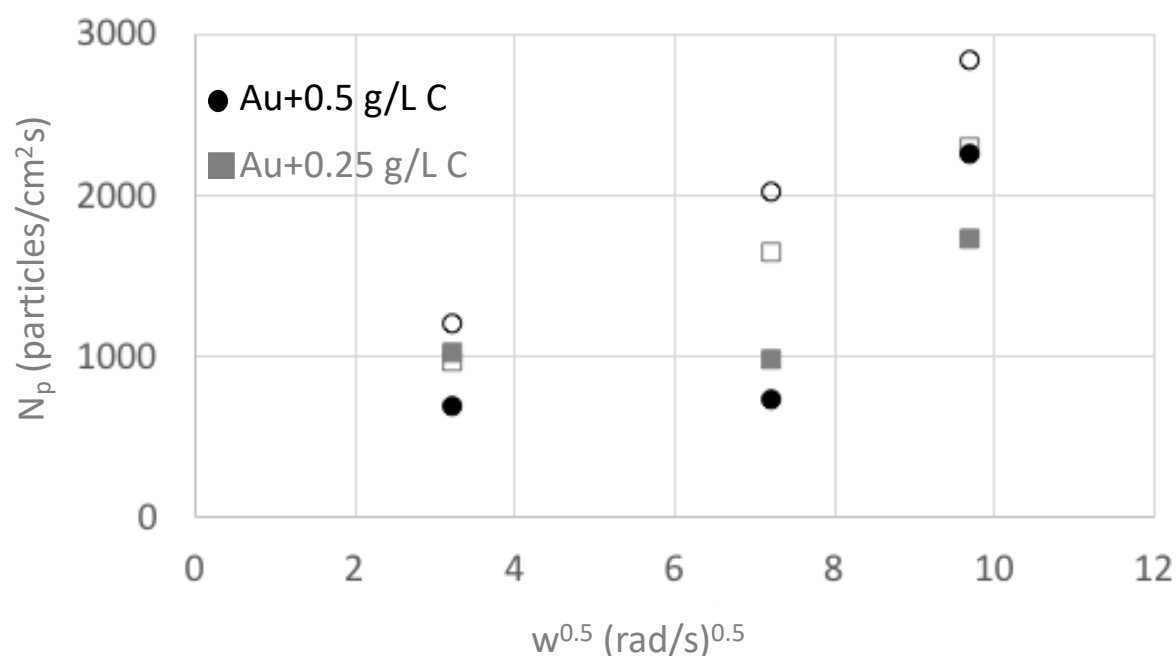


Figure 13. Experimental (bold) and predicted (not filled) incorporation rate by the model as a function of rotation rate of the Ni working electrode with a bulk concentration of 0.25 g/L and 0.5 g/L of C nanocapsules at a current density of  $-1.7 \text{ mA/cm}^2$ .